Proceedings of ASME Turbo Expo 2016: Turbomachinery Technical Conference and Exposition
GT2016
June 13 – 17, 2016, Seoul, South Korea

GT2016-57620

EVALUATION OF RECENT DATA FROM THE SANDIA NATIONAL LABORATORIES CLOSED BRAYTON CYCLE TESTING

Jim Pasch, Matt Carlson, Darryn Fleming, Gary Rochau
Sandia National Labs
Albuquerque, New Mexico, USA

ABSTRACT

At Sandia National Laboratories (SNL), The Nuclear Energy Systems Laboratory / Brayton Lab has been established to research and develop subsystems and demonstrate the viability of the closed Brayton cycles (CBC), and in particular, the recompression CBC. The ultimate objective of this program is to have a commercial-ready system available for small modular reactors. For this objective, R&D efforts must demonstrate that, among other things, component and the system behavior is understood and control is manageable, and system performance is predictable. Research activities that address these needs include investigating system responses to various anticipated perturbations, and demonstrating that component and system performance is understood. To these ends, this paper presents system response to a perturbation, and turbomachinery performance results during steady state operation. A long duration test, with an extensive period at steady state, was completed in the simple CBC configuration. During this period, a cooling perturbation was initiated. Data from this test are presented and evaluated to explain the sequence of events following the perturbation. It was found that a cascading series of events ensued, starting with the fluid condensing effect of the cooling perturbation. The explanation of events emphasizes the highly interactive and nonlinear nature of CBC's. The comparisons of measured and predicted turbomachinery performance yielded excellent results and give confidence that the predictive methods originally envisioned for this system work well.

INTRODUCTION

The DOE Small Modular Reactors (SMR) program completed the development, installation, and commissioning of a megawatt-class supercritical carbon-dioxide (sCO_2) recompression closed Brayton cycle (RCBC) Test Assembly (TA) in July 2012 [1]. The TA was developed to investigate the key technical issues for this power cycle, and to confirm the model estimates of system performance. The TA is designed to operate at 811 K, with rotor speeds of 75,000 rpm, a 1.8 pressure ratio, and total power production of 250 kWe at an efficiency of roughly 30%. The principal objective of the DOE program is to have a commercial-ready RCBC system for SMRs. Exercising the TA throughout its operational envelope, while obtaining the data to evaluate performance, is necessary to convince potential investors of the economic viability of CBC technology. All opportunities to contribute to, and to improve the quality of, these efforts should be considered.

An area of interest that has received little attention and data generation to date is the effects of local perturbations on the system, and the nature of the feedback on system response and stability. Studies of this type guide instrumentation and control (I&C) design considerations. Another continuing area of interest is the quality of predictive capabilities. Understanding the potential quality of predictive performance models is fundamentally important to justifying the use of models to extrapolate and predict the potential commercial viability of the technology.

In support of these two objectives, an sCO_2 CBC, configured in a simple cycle, was operated for an extended period at steady state. During this extended period, a step function perturbation in cooling was imposed to observe the effects around the cycle. Additionally, this test provides an excellent opportunity to compare measured and predicted performance of the turbomachinery.

NOMENCLATURE

CBC	closed Brayton cycle
CO_2	carbon dioxide

h	enthalpy
I&C	instrumentation and control
K	Kelvin
krpm	thousands of rotations per minute
kWe	kilowatt electrical
kWth	kilowatt thermal
$\dot{m}$	mass flow rate
MPa	megapascals
N	rotor shaft speed
P	pressure
PCHE	printed circuit heat exchanger
R&D	research and development
RCBC	recompression closed Brayton cycle
rpm	rotations per minute
sCO_2	supercritical carbon dioxide
SMR	small modular reactor
SNL	Sandia National Laboratories
T	temperature
TA	test assembly
η_c	compressor efficiency
η_t	turbine efficiency
$\eta_{c,map}$	compressor map efficiency
$\eta_{t,map}$	turbine map efficiency

TESTING CONFIGURATION

The SNL TA was configured as a simple CBC. To simplify reconfiguration from the recompression cycle, the low temperature recuperator remained in the circuit. The resulting component and circuit layout is presented in Figure 1. The compressor has design inlet conditions of 59.4 °C and 7791 kPa, and a design point pressure ratio of 1.8. Turbine design inlet conditions are 537.8 °C and 13528 kPa, and a mass flow of 3.14 kg/s. All piping is stainless steel 316. Piping between the low temperature recuperator discharge on the low pressure side, gas cooler, compressor, and low temperature recuperator inlet on the high pressure side is 2 inch schedule 160, providing a flow diameter of 4.29 cm. All other piping is 3 inch schedule 160, giving a flow diameter of 6.68 cm.

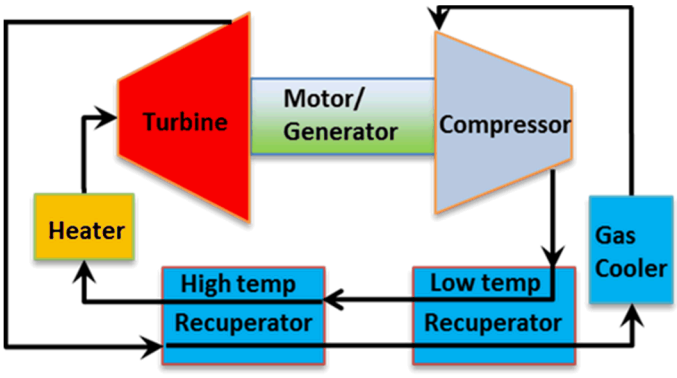

Figure 1: Component and circuit layout for testing.

Heat input is accomplished with six electrically powered immersion heaters connected in series, with 780 kWe combined power capacity. Heat is rejected from the cycle through a printed circuit heat exchanger (PCHE) with water as the cooling fluid, providing 560 kWth heat removal capacity. Both recuperators are also PCHE's, with design point heat transfer duties of 2300 kW and 1700 kW for the high temperature and low temperature recuperators, respectively.

Three sensors are used in various places around the loop. The pressure transducers are high accuracy Honeywell model FP2000 FPA1DN-1Y-2Y-5B-6A. Their output is 4—20 mA that is measured by NI cFP-AI-111 DAQs. The temperature sensors are Conax RTDs, model MRTD4354 that are measured with NI cFP-RTD-124 DAQs. The flow meters measure both flow rate and fluid density. They are Micro Motion Coriolis type, model DH150S and have model 2700 transmitters. Pressure and temperature instruments are installed at the inlet and discharge of all major components. Flow and density measurements are made immediately upstream of the compressor inlet.

The current output of each pressure transducer is assumed linear between 4 and 20 mA. The high accuracy model is installed throughout the system with a 0.10% of full-scale uncertainty (accuracy) rating. The sensor range is 0—20.685 MPa, giving an uncertainty of 20.68 kPa.

The DAQ for this device has several uncertainty sources listed below:

nonlinearity: 0.0015%
offset: 0.1 µA
offset error drift: 20 nA/°C
gain error: 0.03% @ 25°C
gain drift: 40 ppm/°C
resolution: 16-bits

For the sake of brevity, the result of the uncertainty propagation throughout the pressure measurement and processing is given below.

$$U_P = \sqrt{(0.000300P)^2 + (3.00\ \text{psi})^2} \qquad (1)$$

For the conditions discussed in this paper, pressure measurement uncertainty is 20.9 kPa in the low pressure leg, and 21.0 kPa in the high pressure leg.

The temperature sensors are Class A RTDs. The uncertainty of the RTD is

$$U_{RTD} = 0.15 + 0.002T \qquad (2)$$

where T is the measured temperature in degrees Celsius. The NI cFP-RTD-124 DAQs were used to measure the RTDs. System DAQs remain between 15 and 35°C, which results in

lower uncertainty. There are two maxima that depend on the measured temperature range. For temperatures between -200 and 150°C, it is 0.25°C. And for those between 150 and 850°C, it is 0.50°C. The resulting temperature uncertainty is the piecewise function

$$U_T = \begin{cases} \sqrt{(0.15℃ + 0.002T)^2 + (0.25℃)^2} & \text{if } -200℃ < T \leq 150℃ \\ \sqrt{(0.15℃ + 0.002T)^2 + (0.50℃)^2} & \text{if } 150℃ < T \leq 850℃ \end{cases} \quad (3)$$

For the conditions discussed in this paper, temperature measurement uncertainties at the compressor and turbine inlet and outlet range between 0.33 – 0.35 °C, and 1.00 – 1.10 °C, respectively.

The flowmeters are used to measure both flow rate and density. The accuracy of the flowmeter is different with liquids and gasses. Since sCO_2 has properties somewhere between a liquid and a gas, the larger uncertainty for gas values were conservatively used. In cases other than low flow rates, the accuracy of flow rate, with the model 2700 transmitter with MVD technology, is 0.65% of the measured rate. The repeatability is 0.30% of the measured rate. The zero stability is 32.6 kg/hr.

In low flow conditions, when the measured flow rate $\dot{m}$<5000 kg/hr, the uncertainty is nonlinear and fitted with an appropriate relation. There is also a temperature effect on the zero for the flow meter. If the operating temperature is different from that when the zeroing was performed, an uncertainty of 0.01% of nominal flow rate per degree Celsius is estimated. The result is a piecewise relationship for mass flow, given below.

$$U_{\dot{m}} = \begin{cases} \sqrt{(3{,}996\dot{m}^{-1.024})^2 + (0.0030\dot{m})^2 + \left(32.6\frac{\text{kg}}{\text{hr}}\right)^2 + \frac{\left(3.814\frac{kg}{hr}\right)}{℃}|T - T_{\text{zeroed}}|} & if \ \dot{m} < 5000 \text{ kg/hr} \\ \sqrt{\dot{m}^2(0.0065^2 + 0.003^2) + \left(32.6\frac{\text{kg}}{\text{hr}}\right)^2 + \frac{\left(3.814\frac{kg}{hr}\right)}{℃}|T - T_{\text{zeroed}}|} & if \ \dot{m} \geq 5000 \text{ kg/hr} \end{cases} \quad (4)$$

For the conditions discussed in this paper, the mass flow measurement uncertainty is nearly constant at 0.014 kg/s.

The flow meters also measure fluid density. The uncertainty analysis for this is very straightforward, but only liquid density accuracy is defined. A future work should address the uncertainty for gaseous conditions. The accuracy is defined as 2.0 kg/m^3 and the repeatability as 1.0 kg/m^3. Therefore the density uncertainty is constant at

$$U_\rho = \sqrt{\left(2.0\frac{\text{kg}}{\text{m}^3}\right)^2 + \left(1.0\frac{\text{kg}}{\text{m}^3}\right)^2} = 2.24\frac{\text{kg}}{\text{m}^3} \quad (5)$$

The Taylor Series Method for uncertainty propagation, as developed by Coleman and Steele [2], is used for enthalpy uncertainty propogation. These uncertainty effects are extended to apply to efficiency calculations.

Fluid properties are obtained using the National Institute of Technology and Standards database REFPROP [3,4].

EFFECTS OF COOLING PERTURBATION

Closed Brayton cycles are unique in the degree of interaction and feedback between the high and low pressure streams. This is due to the highly recuperated nature of the cycle, the continuous path of pressure communication in a closed volume, and the direct coupling of turbine and compressor. Recuperation imposes thermal nonlinearity, the continuous closed path imposes a momentum nonlinearity, and the turbomachinery coupling establishes direct communication – through the rotor shaft – of operational changes between the hottest and coldest points in the cycle. As the momentum and energy equations are inter-related, events that primarily affect one thermodynamic property will also affect other properties. This coupling between thermal and pressure events can be amplified if the cycle operates with the working fluid near highly nonlinear states, such as the critical point.

Initiating events that impact thermal or pressure conditions at any location in the cycle will affect conditions throughout. The strong feedback action will impact conditions at the initiating location. How the feedback affects conditions throughout the circuit is of interest for system control and varies with specific circumstances. Understanding these interactions, how and at what rate they manifest throughout the closed circuit, how each major component reacts, and effects on performance are of fundamental importance. Instrumentation and control functional requirements will rely on this understanding. Specifications for instruments, such as sensitivity, response rate, placement, and redundancy will be derived, as will specifications for appropriate control response, valves and actuators, and cooling and heating function responses.

An extended duration of steady state conditions was established beginning at about 8000 seconds into the test. Steady operating conditions were established for compressor inlet temperature, heater discharge temperature, and rotor speed. These parameters were maintained at 36.7 °C ±0.35 °C, 415.6 °C ±0.15 °C, and 50 krpm, respectively. Heat loss from the heater discharge to turbine inlet results in a consistent temperature decline of 11.2 °C, yielding a consistent turbine inlet temperature of 404.4 °C.

Effects from a sCO_2 simple closed Brayton cycle heat rejection perturbation are presented below. At the time of perturbation initiation, the system had been at steady state for over 4000 seconds. For this reason, the plots that pertain to this transient

focus on the 100 seconds before and after the initiating event. The perturbation is initiated as a controlled, step increase in cooling water flow through the heat rejection gas cooler. The perturbation begins at 12121 seconds into the test by closing a water supply bypass valve from 66% open down to about 50%, thus forcing more water through the cooler. The bypass valve was returned by a step change to pre-perturbation levels at about 12153 seconds, resulting in increased cooling for 32 seconds. The water valve actuation and effect on compressor inlet temperature immediately downstream of the cooler can be seen in Figure 2 below.

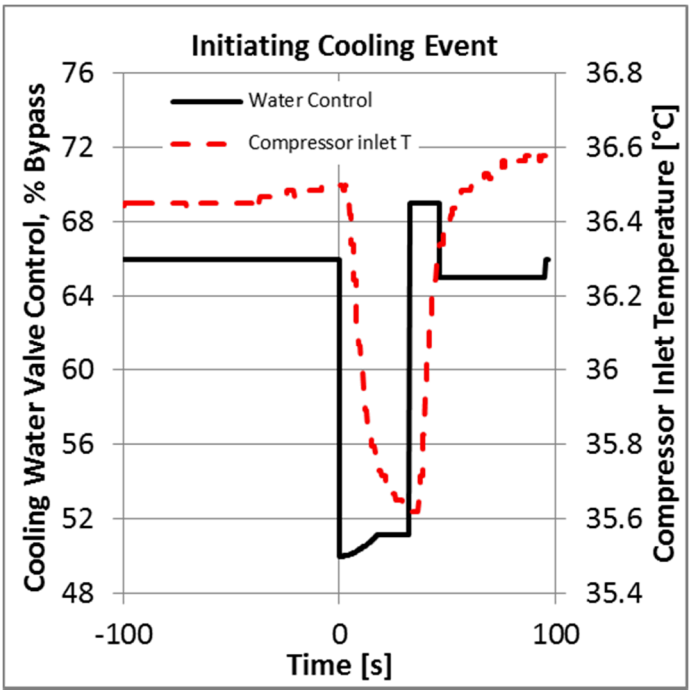

Figure 2: Cooling perturbation event and effect on compressor inlet temperature.

It is seen from this figure that the effect on compressor inlet temperature of both the initiating cooling event, and the return to pre-perturbation levels, is a very rapid initial response. The trace shows an exponential decay in response with time, as is expected.

The compressor inlet CO_2 begins to show signs of cooling at about 3.5 seconds after the initiating event. The effects are observed in inlet temperature and measured density, presented in Figure 3. Temperature declines by 0.9 °C, from 36.5 °C down to 35.6 °C over the period of increased heat rejection. Measured density increases by a rather modest 1.5 kg/m^3.

Operating conditions begin to show significant effects about 5 seconds into the perturbation. Turbo-alternator-compressor (TAC) speed increases by about 330 rpm and net power increases by 0.9 kWe, as presented in Figure 4. Note that the power measurement is scaled such that power into the TAC for motoring is recorded as positive, and power from the TAC from generating is negative power. The speed increase is a function of the controller algorithm which defines a dead-band of speed variation from the commanded speed. In an operational power plant, this magnitude of speed change would not be allowed given that the frequency range is constrained to a very small range centered at 60 Hz.

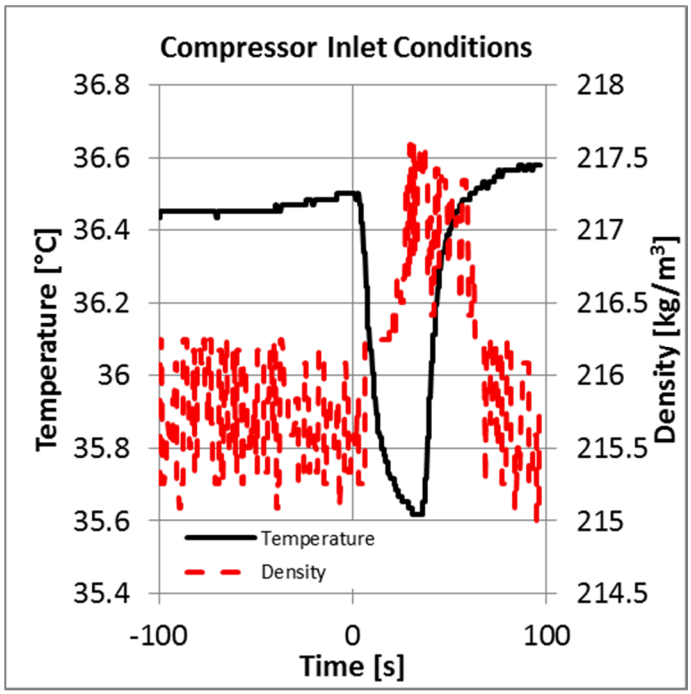

Figure 3: Effects of cooling event on compressor inlet temperature and density.

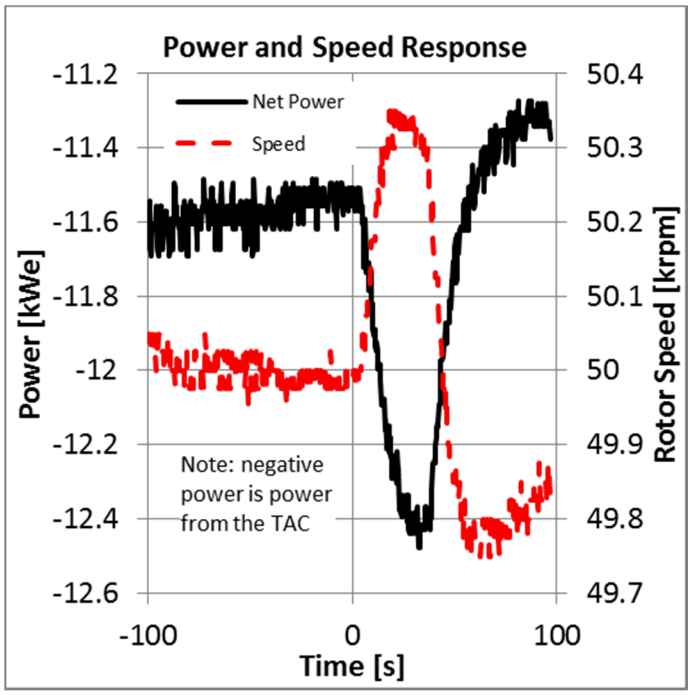

Figure 4: Effects on net TAC power and rotor shaft speed.

It is interesting to compare cycle responses to commanded and thermal-hydraulically initiated speed changes. Commanded speed changes are accomplished by changing the electrical load on the rotor. For speed increases, a temporary load decrease allows the rotor to accelerate. For speed decreases, a temporary load increase causes rotor deceleration. The relative initial effects on speed and power changes for commanded speed changes are opposite to the effects caused by thermal-hydraulic events. The final impact of commanded speed changes on net power production depends on the initial and final operating points of the turbine and compressor, and effects of windage. Commanded speed changes may move the turbomachinery operating points to a more or less efficient point, resulting in more or less generated power.

The increased power output is primarily a result of conditions around the circuit that increase pressure ratio. Pressures in the low pressure leg decrease at 2.8 seconds while those in the high pressure leg increase at 5.0 seconds, as shown in Figure 5 and Figure 6. The magnitude of change is 30 kPa reduction and 30 kPa increase, respectively, giving a net pressure ratio increase of 60 kPa.

The timing of the pressure changes in the low and high pressure legs is important to explaining the event. Additional CO_2 cooling condenses it, and in so doing, decreases the pressure at the cooler. Effects of decreasing pressure transmit throughout the low pressure leg at the speed of sound, all the way back to the turbine discharge, effectively increasing the pressure ratio across the turbine, and thus, power production. In this event, turbine power increased up to 2.0 kW, from 53 kW to 55 kW, at the peak of the event. Increased turbine power increases rotor shaft speed and compressor work. The increasing compressor work is the cause of the increased pressure in the high pressure leg. The rotor inertia is the primary cause of the 2.2 second delay in pressure response on the high pressure leg relative to the low pressure leg. Thus, the cooling effect causes two events that interact with positive feedback on each other.

The increase in compression work amounts to about 1.0 kW, from 31.7 kW to 32.7 kW. Thus, the net between turbine and compressor work amounts to an additional 1.0 kW of power generation, which nearly matches the 0.9 kW additional power shown in Figure 4. The remaining 0.1 kW can be attribute to increased windage losses associated with the higher rotor speed. It is impressive that such a minor change in density can have such a significant impact on condtions throughout the circuit and on performance.

It is important to note that pressure loss itself does not decline during this event, on either the low pressure or the high pressure legs. In fact, Figure 7 presents the delta pressures on each leg. From this figure, it is seen that pressure loss actually increases by a modest 3 – 4 kPa. This is due to the increased mass flow, also show in Figure 7. Therefore, it is not a decrease in pressure loss that generates greater net power, but rather a lower pressure at the turbine discharge that creates a larger pressure ratio across the turbine, and thus, greater turbine work.

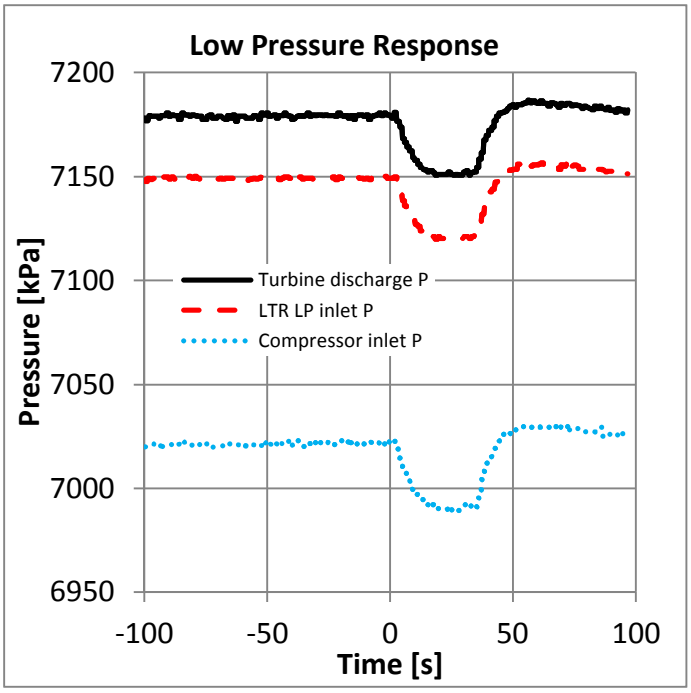

Figure 5: Low pressure leg response to additional cooling.

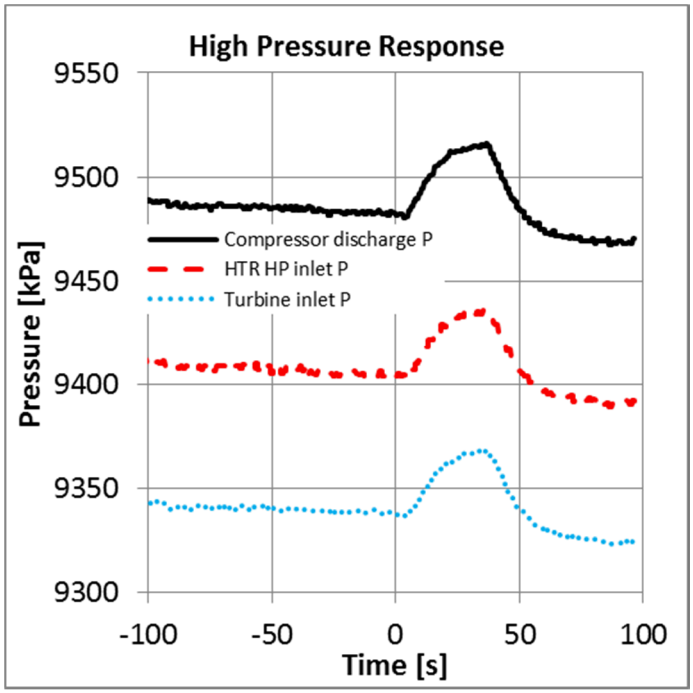

Figure 6: High pressure leg response to additional cooling.

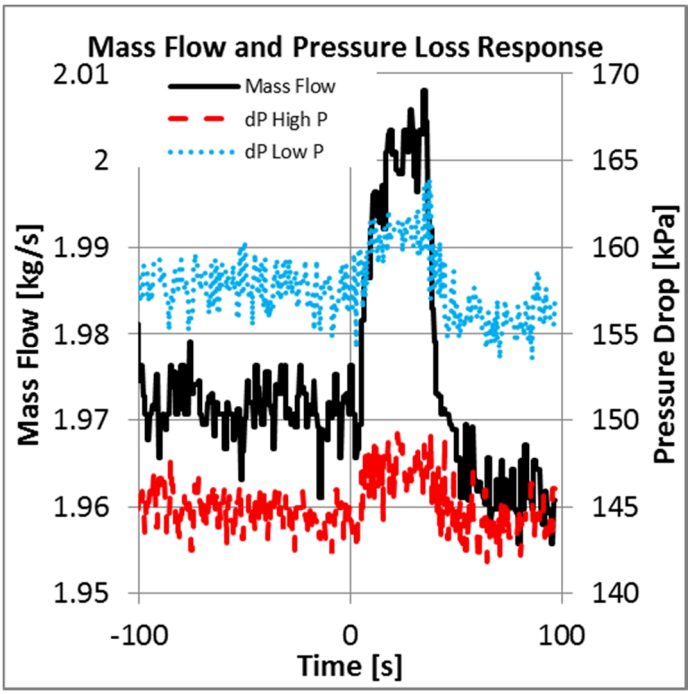

Figure 7: Mass flow and pressure loss response to additional cooling.

Some benefit to reduced compressor power is gained by moving the thermodynamic state of the fluid to a more advantageous condition to reduce specific compressor power. Figure 8 presents this concept graphically as a function of compressor inlet pressure and temperature, given constant compressor efficiency of 80% and discharge pressure of 25 MPa. The region of most rapid variation with respect to pressure and temperature corresponds to the pseudocritical line as defined by the line of maximum specific heat. The conditions presented in Figure 8 are typical for a commercial scale compressor, but the physics applies to the engineering scale compressor in the TA. From this, it is seen that reducing fluid temperature decreases specific power.

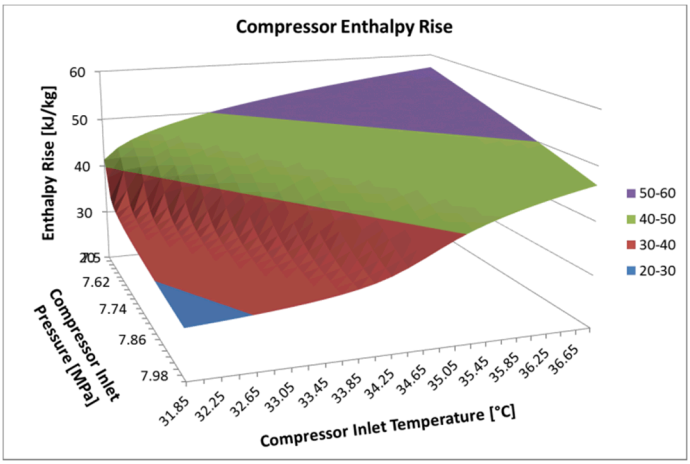

Figure 8: Compressor specific enthalpy rise. Compressor efficiency is 80% and discharge pressure is 25 MPa.

TURBOMACHINERY PERFORMANCE

A benefit of a long duration test at steady state conditions is that extensive turbomachinery data can be obtained with minimal obfuscating effects from transients and thermal inertia. As previously discussed, the long term steady state conditions began around 8000 seconds into the test. The following analysis evaluates turbomachinery predicted and actual performance up to 14000 seconds. This period of time includes the transient discussed previously, at 12121 seconds, the effects of which can be observed in some of the plots.

Compressor efficiency is the ratio of isentropic enthalpy rise to actual enthalpy rise, whereas turbine efficiency is actual enthalpy decrease to isentropic enthalpy decrease,

$$\eta_c = \frac{h_{out,s} - h_{in}}{h_{out} - h_{in}} \qquad \eta_t = \frac{h_{in} - h_{out}}{h_{in} - h_{out,s}} \tag{6}$$

These efficiencies can be calculated from enthalpies determined from measured inlet and discharge temperatures and pressures to give measured efficiencies. They can also be predicted from performance maps to give predicted efficiencies. The functional relations are as follows,

$$\eta_{c,map} = f(T_{in}, P_{in}, \dot{m}, N) \qquad \eta_{t,map} = f(T_{in}, P_{in}, P_{out}, N) \tag{7}$$

In these equations, ṁ is mass flow rate, and N is rotor speed.

Comparisons between measured and map predictions of turbine and compressor efficiencies are presented in Figure 9. The propagated uncertainties for compressor and turbine efficiency calculations in the time period presented in Figure 9 are very stable, with compressor efficiency uncertainties ranging between 0.079 and 0.084, and turbine efficiency uncertainties ranging between 0.048 and 0.049. It is seen that the turbine performance is only about 0.5 percentage points below prediction. Results for the compressor are not quite as good, with differences of about two percentage points towards the end of the steady state period. The magnitude of deviation for the compressor predictions is attributed primarily to two effects. The compressor is operating near the critical point, where small differences between measured and actual thermodynamic conditions can have relatively appreciable effects. Second, the compressor was operating at about 36.7 °C, away from its design point temperature of 59.4 °C. This latter effect impacts the accuracy of the maps, which declines as departure from the design point increases. Still, the uncertainties for both devices encompass predicted performance.

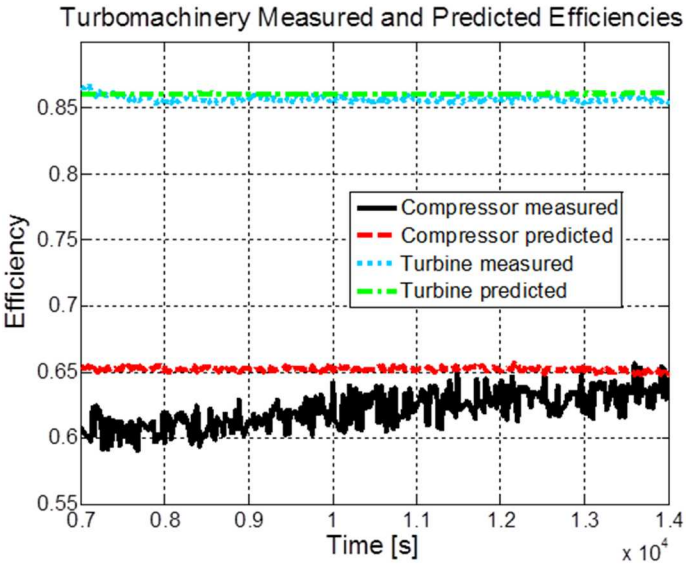

Figure 9: Turbomachinery measured and predicted efficiencies.

The other map predictions for turbomachinery include enthalpy rise in the compressor and mass flow rate in the turbine. The functional dependencies for these two predicted variables are the same as those given for efficiencies in Eqn. 7. Comparison of compressor enthalpy rise prediction with measured is straight forward, as compressor inlet and discharge conditions are measured, from which enthalpy rise can be directly determined. However, comparison of turbine mass flow rate predictions with actual is typically not so straight forward in the dual turbine split flow configuration of the Sandia RCBC. This is because the actual mass flows of the two turbines are not measured. Estimates can be made, based on measured compressor mass flow rates, measured leakage rates, and theoretical flow splits between the two turbines, but inaccuracies and uncertainties are inherently manifest in the calculations. The benefit of the test in this evaluation is that very good knowledge of the actual turbine mass flow is had, given that there is only one turbine, to which flows all of the measured mass flow at the compressor less measured leakage flow.

Results of the map prediction and calculation for turbine mass flow are presented in Figure 10. It is seen that the two traces match for a majority of the time. The difference early in the steady state comparison of about 0.013 kg/s is very small, and is eliminated at about 9000 seconds. Throughout the observed period of time, the difference between measured and predicted mass flow is less than the measurement uncertainty of 0.014 kg/s. Also of interest is the excellent agreement between measurement and prediction during the cooling perturbation at 12121 seconds. This event is manifest as a spike up in mass flow to almost 1.93 kg/s. Note that the difference in measured mass flow between Figure 7 and Figure 10 represents the leakage flow rate through the labyrinth seals that is measured by flow meters in the leakage drain line.

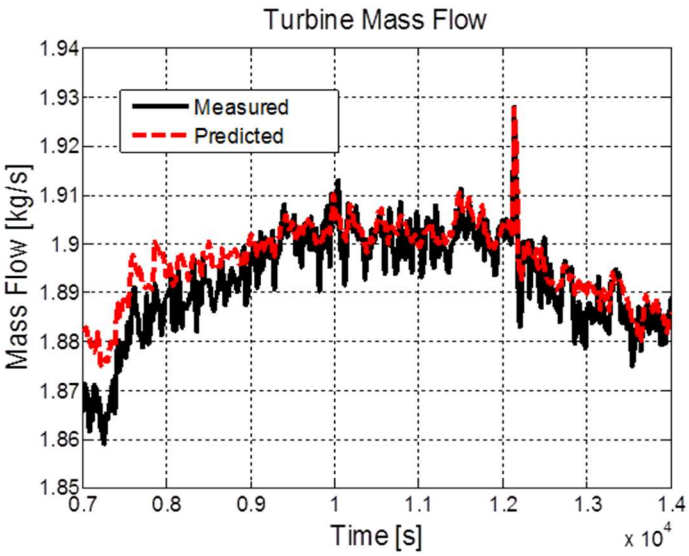

Figure 10: Measured and predicted turbine mass flow.

Analysis of compressor performance is presented in terms of discharge pressure instead of enthalpy, since this is more intuitive. The Compressor measured performance is slightly below prediction, by about 30 kPa for the majority of the period, as show in Figure 11. This falls outside of the pressure measurement uncertainty of 21.0 kPa, and represents an average over-prediction in pressure rise of about 1.2%. While better predictions would most certainly be desired, this is still quite good given the departure from the compressor design operating point and near-critical operating conditions previously discussed. These results also represent some of the best obtained to date.

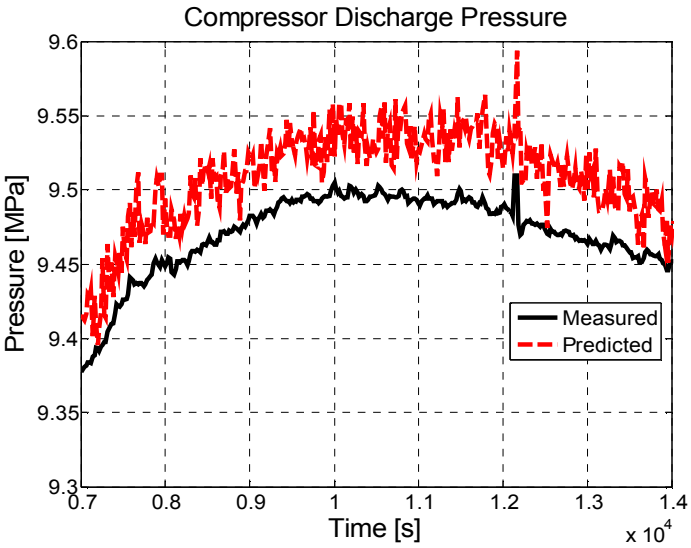

Figure 11: Measured and predicted compressor discharge pressure.

OBSERVATIONS

A step increase in cooling water flow rate following an extended period of steady operation led to a marked response in the system. The additional cooling initiated a series of events that were compound in their effect on system performance. The sequence of effects started with a modest increase in density of about 1.5 kg/m^3, or about 0.7%, at the vicinity of the cooler and compressor. This caused a decrease in pressure that was communicated nearly instantaneously throughout the low pressure leg. The turbine discharge experienced a decrease in back pressure, thus providing for a greater pressure ratio across it, resulting in greater turbine power. The increased turbine power caused the rotor to accelerate and increase speed by 330 rpm. The faster rotor then caused the compressor to perform more work in the form of slightly greater mass flow and greater discharge pressure, which was manifest throughout the high pressure leg. The effects at the compressor that increase pressure ratio and power are consistent with those effects at the turbine, thus generating more power.

Results of the compounding effects are a 2 kW increase in turbine power and 1 kW increase in compressor power. Measured generator power increases by 0.9 kWe, or 7.4%. The remaining 0.1 kWe is attributed to increased windage due to higher rotor speed. The slightly increased mass flow rate caused slightly increased pressure losses in both the low and high pressure legs, but this increased pressure loss was more than offset by the greater pressure ratio.

The observed positive effects for increased cooling are in addition to those resulting from reduced specific compressor power associated with a fluid in a preferred thermodynamic state. Thus, extensive rejection of heat in the cycle, for the conditions considered in this paper, is of great benefit for cycle performance in several ways.

The long duration steady state test, conducted in a simple cycle configuration, afforded a unique opportunity to compare measured and predicted turbomachinery performance. From the results, it was found that turbine predicted performance compared very favorably with measured performance. This is true for both efficiency and mass flow predictions. Efficiencies were generally within 0.5 percentage points, and mass flows matched for most of the steady state operation.

The compressor performance comparisons were not quite as close as those for the turbine. Compressor measured efficiency was lower than prediction by 2 – 3 percentage points for most of the steady state. Measured discharge pressure was about 30 kPa lower than prediction. These results are good given the relatively large departure from the compressor design operating temperature, and operation relatively near the critical point.

CONCLUSIONS

The highly interactive nature of a closed Brayton cycle can lead to system responses to local perturbations that may not be immediately obvious. The feedback to a specific perturbation after the system has reacted may be either compounding or diminishing. How the system responds to various initiating perturbations is of fundamental interest to the design of the I&C subsystem.

The effects of a 32 second heat rejection perturbation during a long duration steady state test were presented and analyzed. The initial effect was decline in pressure on the low pressure leg, causing an increase in turbine work, resulting in increased shaft speed, which caused an increase in compressor work and pressure rise. It was observed that for this particular perturbation, imposed on the particular operating conditions at steady state, the feedback was compounding.

The results from the analysis of the perturbation can be used for developing control responses to such an event. When connected to a grid, it is important to maintain stable conditions throughout the cycle, including rotor speed and generated power. Therefore, rapid and appropriate response to a perturbation is essential to avoid problematic scenarios, including such serious consequences as automatic system trips. The type of testing presented here, and the analytical process employed to characterize the series of events and consequences, can and should be applied to any conceivable perturbation that a commercial system might experience.

The performance of the turbine and compressor were evaluated and compared with predictions. Circumstances for this test were beneficial to know very closely the mass flow rate in the turbine. The measured and predicted values matched for most of the steady state test. The compressor pressure rise was also close to prediction throughout the steady state period. Turbine efficiencies from measurement and prediction were very close together – the best results obtained to date with the TA. Differences in compressor measured and predicted efficiencies were slightly larger than for the turbine, but the causes for these differences are understood and are expected to decrease when the compressor is operated near its design conditions.

The comparisons of measured and predicted turbomachinery performance give confidence that the predictive methods originally envisioned for this system, and employed in other power cycles, can work perfectly well. In particular, the instrumentation and data processing methods employed here are appropriate and adequate for the current needs. These results give confidence in the predictive capabilities of the system models developed at SNL and Argonne National Laboratories and baselined by the SNL CBC testing data.

ACKNOWLEDGMENTS

The authors would like to thank the US Department of Energy – Office of Nuclear Energy. Sandia National Laboratories is a

multi-program laboratory managed and operated by Sandia Corporation, a wholly owned subsidiary of Lockheed Martin Corporation, for the U.S. Department of Energy's National Nuclear Security Administration under contract DE-AC04-94AL85000.

WORKS CITED

[1] Pasch, J., Conboy, T., Fleming, D., & Rochau, G. (2012). *High Temperature Re-Compression Brayton Cycle Design Completion, Delivery, and Commissioning.* Albuquerque, NM: Sandia National Laboratories.

[2] Coleman, H. W., & Steele, W. G. (2009). *Experimentation, Validation, and Uncertainty Analysis for Engineers.* Hoboken: John Wiley & Sons, Inc.

[3] Lemmon, E., Huber, M., & McLinden, M. (2013). *NIST Standard Reference Database 23: reference Fluid Thermodynamic and Transport Properties-REFPROP, Version 9.1.* Gaithersburg: National Institute of Standards and Technology.

[4] Span, R., & Wagner, W. (1996). A New Equation of State for Carbon Dioxide Covering the Fluid Region from the Triple-Point Temperature to 1100 K at Pressure up to 800 MPa. *J. Phys. Chem. Ref. Data*, 25(6):1509-1596.